Impact evaluation of rolling contact fatigue life models [†]

Youngsik Choi[1,*] and Xiaoping Yang[2]

[1]*School of Mechanical Engineering, Chung-Ang University, Seoul, 156-756, Korea*
[2]*Cummins Inc., Columbus, IN 47202, USA*

Abstract

Since the accurate prediction of fatigue life has a significant value, many researchers have attempted to develop a reliable fatigue life model. Recently, rolling contact fatigue life models incorporating machining impact were developed. These models have contributed to a significant improvement in prediction accuracy as compared with earlier models, thus representing a major step forward in the modeling effort. This paper compares the prediction accuracy of these models with that of the prediction method in International Standards. When α is set to 0.25, the observed improvement of prediction accuracy as measured by variance of prediction errors due to these models over that due to prediction method in International Standards is statistically significant. Impact analyses of such improvement are conducted to illustrate its value. It is further noted that while difference was observed between the variance of prediction errors due to the crack initiation life model based on a dislocation model and that due to the crack initiation life model based on a local stress-life curve, the observed difference is not statistically significant.

Keywords: Dislocations; Life prediction; Machining impact; Rolling contact fatigue; Statistics

---

1. Introduction

Since fatigue is one of the most common failure modes for structures subject to cyclic loading, accurate fatigue life prediction has a significant value. Many researchers have attempted to develop a reliable fatigue life model with limited success. The major obstacle for accurate fatigue life prediction is due to a large variance of fatigue life under nominally identical conditions.

With the large variance comes significant uncertainty on fatigue life of nominally identical structures. This significant uncertainty poses great challenges and risks. The challenges include how to properly design, manufacture, and maintain a product prone to fatigue failures under such an uncertainty. The most significant risk is the fatigue failure of a product leading to loss of life, such as fatigue-induced aircraft crashes [1].

The first step for improving fatigue life prediction accuracy is to understand what factors lead to a large variance in fatigue life. While there have been attempts to improve the fatigue life model by using neural network [2, 3], one key finding from previous research [4, 5] is that finish machining processes can have the most significant impact on fatigue performance of machined components by altering residual stress and micro-hardness. It was reported that the variance of machining induced residual stresses influences the fatigue life variance [4] (see Fig. 1).

Based on the aforementioned findings, it is obvious that machining impact should be incorporated into the fatigue life model. Recently, Choi and Liu [6, 7] and Liu and Choi [8] developed rolling contact fatigue life models incorporating residual stress and micro-hardness alterations due to machining processes. Their fatigue life models have contributed a significant improvement in predictive accuracy as compared with earlier models, thus representing a major step forward in the modeling effort.

The objective of this paper is to compare the rolling contact fatigue life model developed by Choi and Liu [6, 7] and the rolling contact fatigue life model developed by Liu and Choi [8] with the Lundberg-Palmgren model [9, 10], on which the prediction method in International Standards [11] is currently based, and to evaluate the impact of these models.

While simple comparison of prediction errors shed light on prediction capability of the models [7-9], such comparison lacks the capability to assess the prediction capability from statistical perspective. Given the inherent large variance of fatigue life and limited number of test samples involved, the assessment of the variance of prediction errors provides critical information to adequately compare prediction capability of fatigue life due to different models.

---

[*]Corresponding author. Tel.: +82 2 820 5721, Fax.: +82 2 814 9476
E-mail address: yycc@cau.ac.kr
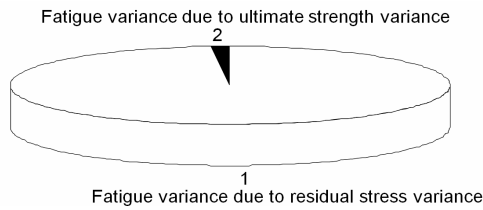
Fig. 1. Fatigue variance due to ultimate strength variance and residual stress variance [4].

Fig. 2. Basquin type log-log straight line S-N relationship.

Another original contribution of this paper is the impact analysis. The impact analysis evaluates what impact on design and maintenance of fatigue critical components the fatigue prediction methods have. This analysis drives home the concept that greater variance of prediction errors leads to bigger design safety factors and shorter maintenance cycle by concrete numbers. This is the price paid for uncertainty.

2. Rolling contact fatigue life models

2.1 Lundberg-Palmgren model

Choi and Liu [7] derived a rolling contact fatigue life model based on Lundberg-Palmgren model so that residual stresses can be incorporated into the model. According to Lundberg-Palmgren model [9, 10], the probability of survival of a volume loaded by a cyclic stress can be expressed as:

$$ln(\frac{1}{s}) \propto \frac{\tau^c N^e V}{Z^h} \tag{1}$$

where s is the probability of survival, τ the maximum orthogonal shear stress, N the number of loading cycles with a probability of survival (s), V the volume at risk, Z the depth at which the maximum orthogonal shear stress occurs, c the stress exponent, e the life exponent, and h is the depth exponent.

Since the maximum orthogonal shear stress does not account for the effect of residual stresses, it is substituted by the maximum shear stress. The previous equation was thus rewritten in terms of the maximum shear stress and solved for the fatigue life as follows:

$$N \propto \left(\frac{Z^h}{\tau_{max}^c V} \right)^{\frac{1}{e}} \tag{2}$$

where τ_{max} is the maximum shear stress, and Z is the depth at which the maximum shear stress occurs.

Since V is proportional to $2alZ$, where a is the half of the contact length, and l is the length of the track, the above equation can be written as:

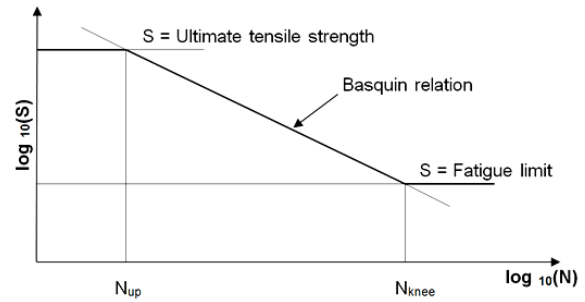$$N \propto \left(\frac{Z^{h-1}}{\tau_{max}^c al} \right)^{\frac{1}{e}}. \tag{3}$$

Accordingly, the final model based on the Lundberg-Palmgren model can be expressed as:

$$N = C' \left(\frac{Z^{h-1}}{\tau_{max}^c al} \right)^{\frac{1}{e}} \tag{4}$$

where C' is the material constant.

This model does not account for the effect of micro-hardness, while residual stresses can be incorporated into the maximum shear stress calculation.

2.2 Choi-Liu model

Choi and Liu [6, 7] proposed a crack initiation life model and a crack propagation life model to predict the initiation of a fatigue spall, and verified the models experimentally. In this paper, the crack initiation life model and the crack propagation life model are combined to predict the fatigue life.

2.2.1 Crack initiation life model

The crack initiation life model was developed by using a local stress-life curve [6, 7]. The Basquin equation [12] is modified according to the local hardness (see Fig. 2). The values for N_{up} and N_{knee} are assumed to be 10^2 and 10^6, respectively. The ultimate tensile strength is estimated based on the local hardness by Eq. (5), and the fatigue limit stress is assumed to be 700 MPa based on the estimate for high strength steel [13].

The crack initiation life model can thus be written as Eq. (6). The crack initiation point is assumed to be where the ratio of maximum shear stress to micro-hardness is highest [14], and the initiation criterion is assumed to be the number of loading cycles required to reach 30 μm length of crack [15].

$$UTS = 3.45(HB) \tag{5}$$

$$N_i = 10^6 \left(\frac{700}{S} \right)^{4/(\log_{10}(UTS)-2.85)} \tag{6}$$

where UTS is the ultimate tensile strength, HB the Brinell hardness, N_i the crack initiation life in loading cycles, and S is the equivalent tensile stress of the maximum shear stress at the crack initiation point.
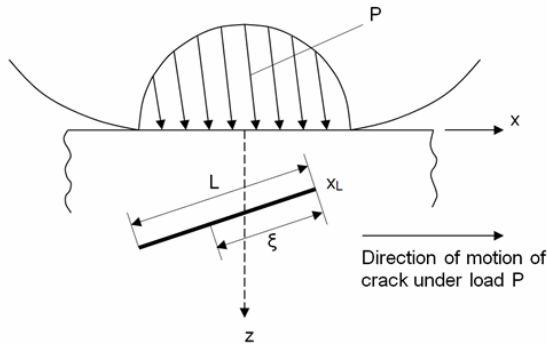
Fig. 3. Geometry of a crack moving under a stationary load.

2.2.2 Crack propagation life model

The crack propagation life model was developed by using the modified Paris' formula [6, 7]. Paris and Erdogan [16] proposed a formula for the correlation between the crack propagation rate and the stress intensity factor range:

$$\frac{da}{dN} = C(\Delta K)^n \tag{7}$$

where a is the half length of the crack, N the number of loading cycles, C the material constant, ΔK the stress intensity factor range, and n is the slope index.

Paris' formula, Eq. (7), is modified, since the crack propagates relatively faster as the local hardness is lower if the stress field is identical [17]:

$$\frac{da}{dN} = C\frac{H_b}{H_l}(\Delta K)^n \tag{8}$$

where H_b and H_l are the Knoop hardness number at the bulk material and the local Knoop hardness number, respectively.

Hearle and Johnson [18] calculated the mode II stress intensity factors at each end of the crack in the half-space, where the stress field over the whole crack is known. The crack geometry used for the calculation of the stress intensity factor is shown in Fig. 3. The corresponding stress intensity factor at the leading tip (K_L) is as follows:

$$K_L = \sqrt{\frac{2}{\pi L}} \int_0^L \tau_c (x_L - \xi)\left\{\frac{L-\xi}{\xi}\right\}^{1/2} d\xi \tag{9}$$

where L is the crack length, τ_c the net shear stress, and x_L is the position of the leading tip.

The net shear stress (τ_c) is the stress available to cause the stress intensities at the crack tip. The driving force for crack propagation in rolling contact has been postulated to be related to the maximum shear stress, and it was experimentally verified [17, 19]. The maximum shear stress is thus assumed to be the net shear stress. The stress intensity factor range is calculated from the variation of K_L at different crack tip positions.

The crack propagation life can be calculated by integrating the crack propagation rate from the initial crack size to the final crack size. The final crack size is derived from the crack size when the crack reaches the surface. The crack propagation life model can then be written as

$$N_p = \int_{a_1}^{a_2} \frac{1}{C\frac{H_b}{H_l}(\Delta K)^n} da \tag{10}$$

where N_p is the crack propagation life in loading cycles, a_1 the half length of the initial crack size, a_2 the half length of the final crack size, and n is the slope index, which is taken as 3 for bearing steels [20].

The half length of the crack can be expressed by using the depth of the leading tip position and the crack propagation angle as follows:

$$a = \frac{z_i - z}{sin\theta} \tag{11}$$

where z_i is the crack initiation depth, z the depth of the leading tip position, and θ is the angle that the crack propagation direction makes with the surface, which is taken as 17.2° based on the experimental observations [14, 21].

2.2.3 Rolling contact fatigue life model

The crack initiation life model and the crack propagation life model are combined to put forward a rolling contact fatigue life model:

$$N = 10^6 \left(\frac{700}{S}\right)^{4/(log_{10}(UTS) - 2.85)} + \int_{a_1}^{a_2} \frac{1}{C\frac{H_b}{H_l}(\Delta K)^n} da \tag{12}$$

where N is the fatigue life in loading cycles.

2.3 Liu-Choi model

The difference between Choi-Liu model [6, 7] and Liu-Choi model [8] is the crack initiation life model.

2.3.1 Crack initiation life model

Liu and Choi [8] developed a crack initiation life model based on a dislocation model. Tanaka and Mura [22] proposed a dislocation model for fatigue crack initiation. The simplified form of the model can be expressed as follows:

$$N_i = \frac{AW_c}{(\Delta\tau - 2\tau_k)^2} \tag{13}$$

where N_i is the number of loading cycles to crack initiation, W_c the specific fracture energy for a unit area, $\Delta\tau$ the range of local shear stress, τ_k the frictional stress, and A is a function
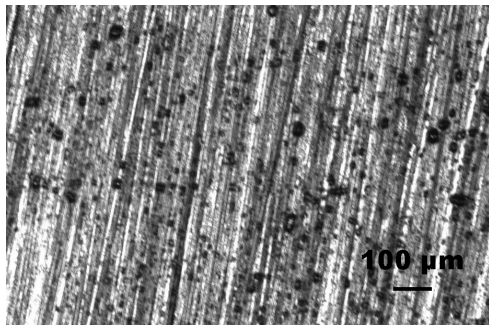
Fig. 4. Cross-sectional view of specimen [8].

Fig. 5. Dimensions of specimen.

depending on the material properties and the type of initial cracks. A can be written as [23]:

$$A = \begin{cases} \dfrac{4G_h}{\pi(1-\nu)l} & \text{along slip bands} \\[2em] \dfrac{2G_h}{l} & \text{along grain boundary} \\[2em] \dfrac{4G_h(G_h+G_i)m^2}{G_i(m+l)^2 R} & \text{along interface of inclusion} \end{cases}$$

(14)

where G_h is the shear modulus of homogeneous media, G_i the shear modulus of inclusion, ν the Poisson ratio, l the semi-length of slip band, m the semi-minor length of elliptical slip band area, and R is the radius of inclusion.

Subsurface cracks typically initiate from inclusions, which act as a stress raiser [24-27]. The inclusions intensify the local stress, and the periphery of the inclusion is strained, eventually initiating cracks [28]. Fractographic examination of high strength steels showed that the initiation sites for subsurface cracks are always inclusions located in the interior of the material [29].

Accordingly, it is assumed that a crack initiates along the interface of the inclusion. To further simplify the model, the semi-length of slip band is assumed to be equal to the semi-minor length of the elliptical slip band area [23, 29]. With these assumptions, the crack initiation life model can be rewritten as:

$$N_i = \frac{G_h(G_h+G_i)W_c}{(\Delta\tau - 2\tau_k)^2 G_i R} \cdot$$

(15)

The local shear stress is replaced by the maximum shear stress based on the previous finding [14]. Based on the measurement of inclusions in Fig. 4 [8], the crack initiating inclusion size is assumed to be 30 µm. Accordingly, the crack initiation life model can be simplified as:
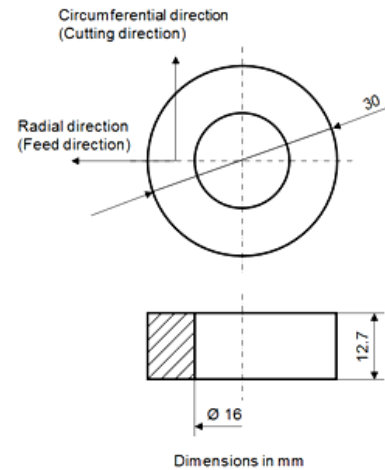
$$N_i = \frac{I}{(\Delta\tau_{max} - 2\tau_k)^2}$$

(16)

where I is the initiation constant ($I = G_h(G_h+G_i)W_c/(G_iR)$) and $\Delta\tau_{max}$ the range of maximum shear stress during a cycle at the initiation point. Accordingly, the crack initiation life can be predicted by using the maximum shear stress at the initiation point, provided that the initiation constant and the frictional stress of the crack initiation life model are determined.

2.3.2 Rolling contact fatigue life model

The developed crack initiation life model was combined with the crack propagation life model [6, 7] to predict the fatigue life as follows:

$$N = \frac{I}{(\Delta\tau_{max} - 2\tau_k)^2} + \int_{a_1}^{a_2} \frac{1}{C\dfrac{H_b}{H_l}(\Delta K_L)^n} da$$

(17)

where N is the fatigue life in number of loading cycles.

3. Experimental

3.1 Specimens for Choi and Liu's study

Specimens of through hardened AISI 1053 and AISI 1070 steels were prepared for the experiment, since these steels are used for bearing applications. The dimensions of the specimen were selected to minimize a deflection by the chucking forces of a standard jaw and to be uniformly through hardened [30]. The selected dimensions are shown in Fig. 5.

The cutting tools used in the experiment were CBN (cubic boron nitride) tools and ceramic tools. The machining conditions, such as tool material, tool nose radius, tool chamfer angle, cutting speed, feedrate, depth of cut, coolant type, and specimen material, were selected according to Taguchi's orthogonal array [31] that was employed to distribute the effect of machining conditions on surface integrity evenly.

Eighteen different combinations of machining conditions were determined, and the specimens were numbered sequen-

tially according to the combinations of machining conditions. Specimen Nos. 1-12 were machined by square tools with a tool nose radius of 0.79 or 1.59 mm, and specimen Nos. 13-18 were machined by round tools with a tool nose radius of 4.76 mm.

Additionally, the specimens were machined at two different cutting tool conditions: new and worn tools. The condition of a new tool is defined as the state of the unused tool, while that of a worn tool is defined as the state of the tool after being used for machining 150 identical specimens at the same machining conditions.

However, specimens 11 and 13 were machined by the tools after 120 specimens and 78 specimens, respectively, were machined, since the tools were broken before machining 150 specimens. All the specimens were machined at a constant surface speed.

3.2 Specimens for Liu and Choi's study

Specimens of through hardened AISI 1053 steel were prepared for the experiment. The dimensions of the specimen were the same as detailed in Section 3.1. The flat surfaces of the specimens were ground in a sequence of three cuts of 51 μm, followed by two cuts of 25 μm, two cuts of 13 μm, and one cut of 5 μm. Gentle grinding conditions were used to induce less thermal damage and less residual stress beneath the ground surface [32].

Subsequently, a layer of 50 μm thickness was removed by an etching to remove a layer that was thermally damaged and had residual stresses due to grinding. The thickness of removed layer by an etching is 10 times the depth of cut of the last pass in grinding. Consequently, specimens having negligible thermal damage and residual stresses induced only by heat treatment were prepared.

3.3 Rolling contact fatigue test for Choi and Liu's study

A special test rig was used to perform rolling contact fatigue tests. These tests were performed in a temperature-controlled room that was set to 25°C. The thrust ball bearing, which has Grade 25 balls of 3.69 mm diameter, was used in the test. This bearing was inserted between two specimens.

The upper specimen was rotated at 1840 rpm, and the lower specimen was fixed in the test rig. An axial load that produces a maximum Hertzian stress (MHS) of 2720 MPa was imposed on the upper specimen. In the case of through hardened AISI 1053 steel, this loading induces a contact area diameter of 79 μm and a maximum shear stress of 843.2 MPa at a depth of 36.9 μm, assuming no friction between the ball and the specimen.

SAE-30 lubrication oil was circulated through a 0.25 μm filtered-pump feed system at a rate of 56.8 cm³/min. The bearing and the specimens were immersed in this lubricant while a test was run. Fig. 6 shows a schematic diagram of the rolling contact fatigue test rig. The experimental lives by this test rig showed less than 10-17% differences with those by the Falex
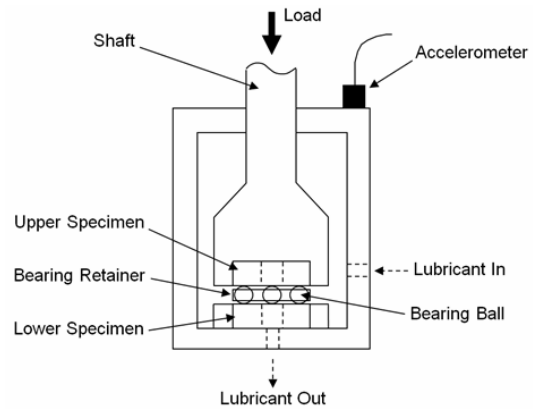

Fig. 6. Schematic diagram of a rolling contact fatigue test rig [7].

multi-specimen rolling fatigue tester [30].

The rolling contact fatigue test was monitored by an accelerometer connected to a vibration meter. The vibration signal, which is influenced by both the upper and lower specimens, was acquired by the data acquisition system during the test. The vibration threshold level was set to 0.2 g to detect the initiation of a fatigue spall. To enable a reliable comparison, this level was fixed for all the tests.

3.4 Rolling contact fatigue test for Liu and Choi's study

Rolling contact fatigue tests were performed at the condition detailed in Section 3.3. However, loading conditions were changed: Axial loads that produce MHS of 1007, 1131, 1262, 1424, 1593, 1848, 2165, 2434, 2724, 3117, 3434, and 3696 MPa were imposed on the upper specimen.

4. Results and discussion

4.1 Prediction of rolling contact fatigue life

The experimental and predicted fatigue life in Choi and Liu's study [7] are listed in Tables 1 and 2, and the experimental and predicted fatigue life in Liu and Choi's study [8] are listed in Table 3: The specimens whose fatigue data were used to derive material constants are not listed. Prediction errors due to various models are also in Tables 1-3.

4.2 Statistical analyses

Statistical analyses have been carried out by using Minitab R14. Summary statistics for prediction errors are listed in Table 4; the P-value was derived by using the Anderson-Darling normality test. It is noted that six of seven errors are not normally distributed. Tests for equal variances for prediction errors are shown from Figs. 7-11. Levene's test results were used if data were not normally distributed. The equal variance test starts with the null hypothesis that the variances between the tested groups are equal. The alternative hypothesis is that all variances are not equal. The p–value of the test is com-

Table 1. Experimental and predicted fatigue life for specimens turned by a new tool.

Specimen	N_e	N_{CL}	N_{LP}	$N_e - N_{CL}$	$N_e - N_{LP}$
1	2.36E+06	3.28E+06	1.03E+07	-9.20E+05	-7.90E+06
2	2.59E+06	4.33E+06	1.04E+07	-1.74E+06	-7.77E+06
4	6.49E+05	1.15E+06	9.54E+05	-5.01E+05	-3.05E+05
5	1.04E+06	1.32E+06	8.06E+05	-2.80E+05	2.34E+05
6	2.37E+06	3.06E+06	8.78E+06	-6.90E+05	-6.41E+06
7	5.96E+06	5.63E+06	4.58E+07	3.30E+05	-3.99E+07
8	9.85E+06	7.51E+06	2.46E+08	2.34E+06	-2.36E+08
9	2.93E+06	3.83E+06	4.19E+07	-9.00E+05	-3.89E+07
10	4.53E+06	2.34E+06	3.24E+07	2.19E+06	-2.78E+07
12	1.48E+06	1.48E+06	1.37E+06	0.00E+00	1.10E+05
14	2.51E+05	1.73E+06	1.32E+05	-1.48E+06	1.19E+05
16	3.24E+06	9.89E+05	3.85E+05	2.25E+06	2.86E+06
17	4.90E+05	1.15E+06	6.81E+05	-6.60E+05	-1.91E+05
18	7.27E+05	6.72E+05	1.98E+05	5.50E+04	5.29E+05

N_e = Experimental fatigue life
N_{CL} = Fatigue life predicted by Choi-Liu model
N_{LP} = Fatigue life predicted by Lundberg-Palmgren model

Table 2. Experimental and predicted fatigue life for specimens turned by a worn tool.

Specimen	N_e	N_{CL}	N_{LP}	$N_e - N_{CL}$	$N_e - N_{LP}$
2	1.42E+06	1.75E+06	7.10E+06	-3.30E+05	-5.68E+06
3	9.83E+06	6.05E+06	4.92E+08	3.78E+06	-4.82E+08
4	2.82E+05	8.24E+05	1.28E+05	-5.42E+05	1.54E+05
5	1.18E+06	1.03E+06	4.54E+06	1.50E+05	-3.36E+06
6	9.34E+05	1.66E+06	9.83E+05	-7.26E+05	-4.92E+04
7	8.23E+05	1.04E+06	2.74E+06	-2.17E+05	-1.92E+06
8	7.65E+06	4.40E+06	2.55E+08	3.25E+06	-2.47E+08
9	9.07E+05	6.05E+05	1.21E+06	3.02E+05	-3.02E+05
10	2.71E+05	7.09E+05	6.84E+04	-4.38E+05	2.03E+05
12	2.70E+05	6.78E+05	1.19E+05	-4.08E+05	1.51E+05
13	4.21E+05	4.68E+05	3.63E+05	-4.70E+04	5.81E+04
14	3.01E+05	2.82E+05	8.75E+04	1.90E+04	2.14E+05
15	1.25E+06	1.52E+06	1.39E+07	-2.70E+05	-1.26E+07
18	4.53E+05	1.01E+06	1.05E+06	-5.57E+05	-6.00E+05

N_e = Experimental fatigue life
N_{CL} = Fatigue life predicted by Choi-Liu model
N_{LP} = Fatigue life predicted by Lundberg-Palmgren model

Table 3. Experimental and predicted fatigue life for ground specimens.

MHS (MPa)	N_e	N_{LC}	N_{CL}	N_{LP}	$N_e - N_{LC}$	$N_e - N_{CL}$	$N_e - N_{LP}$
1131	2.70E+07	2.32E+07	N/A	9.59E+07	3.85E+06	N/A	1.94E+07
1262	1.39E+07	1.33E+07	N/A	3.20E+07	6.00E+05	N/A	7.86E+06
1424	8.37E+06	7.67E+06	8.35E+06	9.21E+06	7.00E+05	1.79E+04	7.61E+05
1593	4.75E+06	4.74E+06	4.57E+06	2.85E+06	1.00E+04	1.78E+05	-3.17E+06
1848	3.56E+06	2.57E+06	2.08E+06	7.12E+05	9.90E+05	1.48E+06	-1.42E+07
2165	2.23E+06	1.52E+06	1.04E+06	2.23E+05	7.13E+05	1.19E+06	-2.01E+07
2434	1.42E+06	1.05E+06	6.56E+05	7.10E+04	3.70E+05	7.64E+05	-2.70E+07
2724	1.07E+06	7.39E+05	4.25E+05	2.25E+04	3.31E+05	6.45E+05	-4.99E+07
3117	7.23E+05	5.41E+05	3.08E+05	5.78E+03	1.82E+05	4.15E+05	-8.97E+07
3434	5.29E+05	4.62E+05	2.76E+05	2.12E+03	6.70E+04	2.53E+05	-1.32E+08

N_e = Experimental fatigue life
N_{LC} = Fatigue life predicted by Liu-Choi model
N_{CL} = Fatigue life predicted by Choi-Liu model
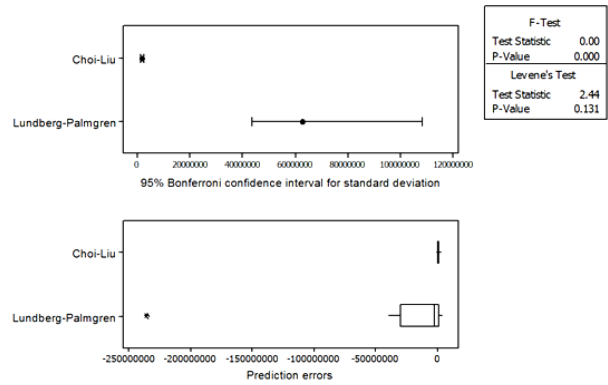N_{LP} = Fatigue life predicted by Lundberg-Palmgren model

Fig. 7. Test for equal variances for prediction errors between Choi-Liu model and Lundberg-Palmgren model (specimens turned by a new tool).
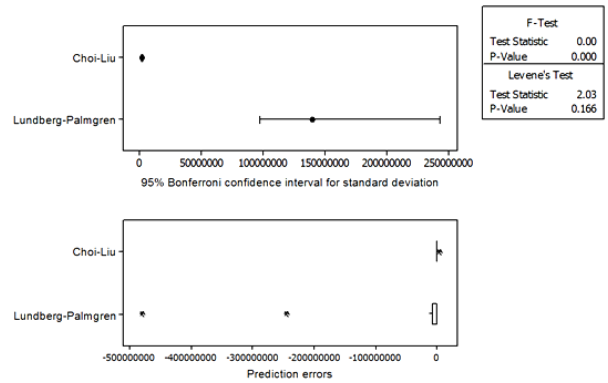

Fig. 8. Test for equal variances for prediction errors between Choi-Liu model and Lundberg-Palmgren model (specimens turned by a worn tool).
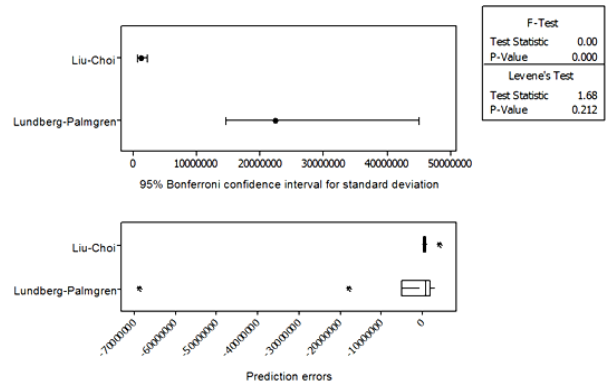

Fig. 9. Test for equal variances for prediction errors between Liu-Choi model and Lundberg-Palmgren model (ground specimens).

pared against α value to decide whether to accept the null hypothesis or reject the null hypothesis. If the p–value is less than α, the null hypothesis is rejected. For the purpose of this study, α is set as 0.25.

Fig. 7 has a p–value of 0.131, Fig. 8 has a p–value of 0.166, Fig. 9 has a p–value of 0.212, and Fig. 10 has a p–value of 0.122. All p–values are smaller than α (0.25), which means that the null hypothesis is rejected for all cases. The conclu-
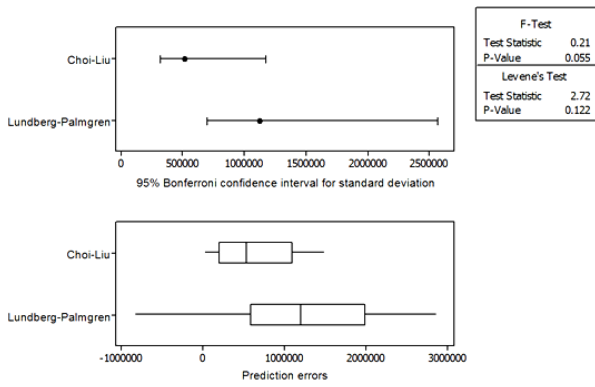
Fig. 10. Test for equal variances for prediction errors between Choi-Liu model and Lundberg-Palmgren model (ground specimens).
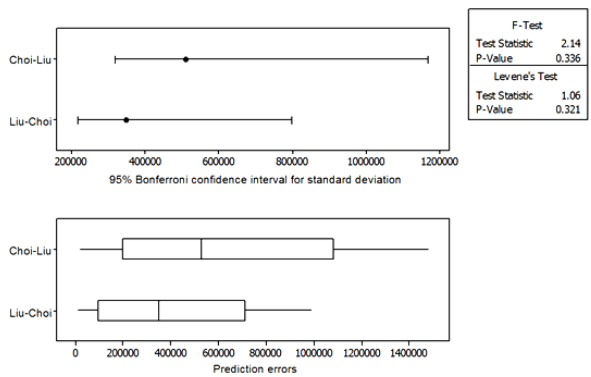

Fig. 11. Test for equal variances for prediction errors between Liu-Choi model and Choi-Liu model (ground specimens).

Table 4. Summary statistics for prediction errors.

	P-value	Mean	Median	95% confidence interval for mean	95% confidence interval for median
N_e - N_{CL} (NT)	0.027	-429	-390500	[-777740, 776882]	[-901029, 425726]
N_e - N_{LP} (NT)	0.005	25808857	-3357500	[-61767140, 10149425]	[-28371268, 124919]
N_e - N_{CL} (WT)	0.005	283286	-243500	[-526349, 1092920]	[-443352, 157823]
N_e - N_{LP} (WT)	0.005	-53766507	-451000	[-134324878, 26791864]	[-6036142, 151154]
N_e - N_{LC} (G)	0.005	781300	485000	[-21716, 1584316]	[142631, 807829]
N_e - N_{CL} (G)	0.615	617863	530000	[191524, 1044201]	[167697, 1208663]
N_e - N_{LP} (G)	0.005	-7743300	883500	[-23731030, 8244430]	[-6746856, 1937658]

NT = new tool, WT = worn tool, G = ground

Table 5. Scenario one impact analysis.

	Predicted life	95LEM	95LML	Inspection interval	Target fatigue life	Design safety factor
Choi-Liu	7.50E+06	-4.43E+05	7.06E+06	7.06E+06	3.00E+06	2.35
Lundberg-Palmgren	7.50E+06	-6.03E+06	1.46E+06	1.46E+06	3.00E+06	0.49

95LEM = 95% confidence interval lower error median
95LML = 95% confidence interval lower median life

sion is that all variances are not equal. Fig. 7 shows that the variance of prediction errors for fatigue life of samples turned by a new tool due to Choi-Liu model is smaller than that due to Lundberg-Palmgren model. Fig. 8 shows that the variance of prediction errors for fatigue life of samples turned by a worn tool due to Choi-Liu model is smaller than that due to Lundberg-Palmgren model. Fig. 9 shows that the variance of prediction errors for fatigue life of ground samples due to Liu-Choi model is smaller than that due to Lundberg-Palmgren model. Fig. 10 shows that the variance of prediction errors for fatigue life of ground samples due to Choi-Liu model is smaller than that due to Lundberg-Palmgren model. In testing the equal variances for prediction errors between Lundberg-Palmgren model and Choi-Liu model for ground specimens, the prediction errors corresponding to MHS from 1424 MPa to 3434 MPa were used in order to be consistent between the models.

Fig. 11 has a p–value of 0.321, which is greater than 0.25, hence the null hypothesis stays. It means that the variance of prediction errors for fatigue life due to Choi- Liu model and that due to Liu–Choi model are statistically equal. Again, the prediction errors corresponding to MHS from 1424 MPa to 3434 MPa were used in order to be consistent between the models.

4.3 Scenario one impact analysis

Impact analysis was performed to compare Choi-Liu model and Lundberg-Palmgren model. It is assumed that the prediction errors for both Choi-Liu model and Lundberg-Palmgren model follow the distributions shown in Table 4. Since the distributions are not normal, the predicted life is treated as a median value. The predicted life for both models is assumed to be $7.50X10^6$.

The impact analysis results are summarized in Table 5. With 95% confidence interval for median, the lower median life is $7.06X10^6$ for Choi-Liu model and $1.46X10^6$ for Lundberg-Palmgren model. It thus indicates that the inspection interval for Choi-Liu model is almost 5 times longer than that for Lundberg-Palmgren model if the inspection interval is determined based on 95% confidence interval.

If the target fatigue life is $3.00X10^6$, the design safety factor achieved is 2.35 for Choi-Liu model and 0.49 for Lundberg-Palmgren model. Since the design safety factor of 0.49 is not acceptable, the designer who predicts a fatigue life by using Lundberg-Palmgren model has to redesign. If the designer needs to achieve the design safety factor of 2.35, the design should be reinforced significantly so that the predicted mean fatigue life reaches $1.31X10^7$.

Since both models predict an identical component, the ac-

Table 6. Scenario two impact analysis.

	Target safety factor	Target fatigue life	95LEM	PLT	Design safety factor
Liu-Choi	2	3.00E+06	1.43E+05	2.86E+06	1.90
Lundberg-Palmgren	2	3.00E+06	-6.75E+06	9.75E+06	6.50

95LEM = 95% confidence interval lower error median
PLT = Predicted life for target fatigue life

tual fatigue life does not change with the fatigue life model used for prediction. However, due to the larger uncertainty of Lundberg-Palmgren model, extra inspections and design reinforcement should be performed to meet desired reliability, which leads to significant waste and reduced competitiveness.

4.4 Scenario two impact analysis

Impact analysis was performed to compare Liu-Choi model and Lundberg-Palmgren model. It is assumed that the prediction errors for both models follow the distributions shown in Table 4. Additionally, it is assumed that the target safety factor in terms of fatigue life is 2, and the target fatigue life is 3.00×10^6.

The impact analysis results are summarized in Table 6. If decisions are made based on 95% confidence interval, the design safety factor needs to be 1.9 if the fatigue life is predicted by Liu-Choi model, while it needs to be 6.5 if the fatigue life is predicted by Lundberg-Palmgren model. This is the price to pay for larger uncertainty due to Lundberg-Palmgren model.

In this paper, Lundberg-Palmgren model could account for the effect of residual stresses by replacing the maximum orthogonal shear stress with the maximum shear stress. However, it does not account for the effect of micro-hardness, which can partly explain worse prediction accuracy.

While both residual stresses and micro-hardness affect the rolling contact fatigue life, the effect of residual stresses is more significant than that of micro-hardness [6]. It is thus conceivable that Lundberg-Palmgren model shows its inherent limitations in predicting fatigue life.

5. Conclusions

The experimental fatigue lives analyzed by using the rolling contact fatigue life models incorporating machining impact yielded the following conclusions.

When α is set as 0.25, tests of equal variances for prediction errors indicate that both Choi-Liu model and Liu-Choi model yield smaller variances of prediction errors than those due to Lundberg-Palmgren model statistically. In the same time, the variance of prediction errors for fatigue life due to Choi- Liu model and that due to Liu –Choi model are statistically equal. The variance of prediction errors is an important measure of

prediction accuracy as it concerns the uncertainty of the prediction results. Impact analyses are conducted to illustrate its value.

To achieve the same level of reliability, the inspection interval should be shorter and the design safety factor should be larger in the case of Lundberg-Palmgren model than those of Choi-Liu model or Liu-Choi Model because Lundberg-Palmgren model induces higher prediction errors.

In the impact analysis to compare Choi-Liu model and Lundberg-Palmgren model, it is noted that the inspection interval for Choi-Liu model is almost 5 times longer than that for Lundberg-Palmgren model assuming that the inspection interval is determined based on 95% confidence interval.

If the target fatigue life is 3.00×10^6, the design safety factor is 2.35 for Choi-Liu model and 0.49 for Lundberg-Palmgren model, which indicates that the design should be reinforced significantly if a fatigue life is predicted by using Lundberg-Palmgren model.

In the impact analysis to compare Liu-Choi model and Lundberg-Palmgren model, it is noted that a design safety factor of 6.5 is needed for the fatigue life prediction based on Lundberg-Palmgren model, while a design safety factor of less than 2 is needed for the fatigue life prediction based on Liu-Choi model if decisions are made based on 95% confidence interval.

Therefore, it is conceivable that the benefits gained by Choi-Liu model or Liu-Choi model over Lundberg-Palmgren model, on which the prediction method in International Standards is currently based, are evident.

Acknowledgment

References

[1] X. Yang, *A methodology for predicting the variance life incorporating the effects of manufacturing processes*, Ph.D. Thesis, Purdue University (2001).

[2] S. Cho and W. Joo, A study on fatigue crack growth and life modeling using backpropagation neural networks, *Transactions of the Korean Society of Mechanical Engineers* A, 24 (2000) 634-644.

[3] D. W. Lee and S. H. Hong, A study on fatigue damage modeling using neural networks, *Journal of Mechanical Science and Technology*, 19 (2005) 1393-1404.

[4] X. Yang and C. R. Liu, A methodology for predicting the variance of fatigue life incorporating the effects of manufacturing processes, *Journal of Manufacturing Science and Engineering*, 124 (2002) 745-753.

[5] X. Yang, C. R. Liu and A. F. Grandt, An experimental study on fatigue life variance, residual stress variance, and their correlation of face-turned and ground TI 6AL-4V samples, *Journal of Manufacturing Science and Engineering*, 124

(2002) 809-819.

[6] Y. Choi and C. R. Liu, Rolling contact fatigue life of finish hard machined surfaces: Part 1. Model development, *Wear*, 261 (2006) 485-491.

[7] Y. Choi and C. R. Liu, Rolling contact fatigue life of finish hard machined surfaces: Part 2. Experimental verification, *Wear*, 261 (2006) 492-499.

[8] Y. Choi and C. R. Liu, A new methodology for predicting crack initiation life for rolling contact fatigue based on dislocation and crack propagation, *International Journal of Mechanical Sciences*, 50 (2008) 117-123.

[9] G. Lundberg and A. Palmgren, Dynamic capacity of rolling bearings, *Acta Polytechnica Mechanical Engineering Series*, 1 (1947) 3.

[10] G. Lundberg and A. Palmgren, Dynamic capacity of rolling bearings, *Acta Polytechnica Mechanical Engineering Series*, 2 (1952) 4.

[11] International standards organization, Rolling bearings-dynamic load ratings and rating life: Part 1. Calculation methods, *International Standard*, 281/1-1977 (E).

[12] O. H. Basquin, The experimental law of endurance tests, *ASTM*, 10 (1910) 625-630.

[13] R. I. Stephens, A. Fatemi, R. R. Stephens and H. O. Fuchs, *Metal fatigue in engineering*, Wiley-Interscience, New York, USA (2001).

[14] X. Leng, Q. Chen and E. Shao, Initiation and propagation of case crushing cracks in rolling contact fatigue, *Wear*, 122 (1988) 33-43.

[15] E. Bormetti, G. Donzella and A. Mazzu, Surface and sub-surface cracks in rolling contact fatigue of hardened components, *Tribology Transactions*, 45 (2002) 274-283.

[16] P. Paris and F. Erdogan, A critical analysis of crack propagation laws, *Journal of Basic Engineering* (1963) 528-534.

[17] Q. Chen, X. Leng and E. Shao, Influence of microstructure and residual stress on the stages of case crushing, *Wear*, 122 (1988) 45-55.

[18] A. D. Hearle and K. L. Johnson, Mode II stress intensity factors for a crack parallel to the surface of an elastic half-space subjected to a moving point load, *Journal of Mechanics and Physics of Solids*, 33 (1985) 61-81.

[19] B. Jiang, X. Zheng and M. Wang, Calculation for rolling contact fatigue life and strength of case-hardened gear materials by computer, *Journal of Testing and Evaluation*, 21 (1993) 9-13.

[20] B. L. Averbach, Fracture of bearing steels, *Metal Progress*, December (1980).

[21] S. R. Agha, *Fatigue performance of superfinish hard turned surfaces in rolling contact*, Ph.D. Thesis, Purdue University (2000).

[22] K. Tanaka and T. Mura, Dislocation model for fatigue crack initiation, *Journal of Applied Mechanics*, 48 (1981) 97-103.

[23] R. S. Zhou, H. S. Cheng and T. Mura, Micropitting in rolling and sliding contact under mixed lubrication, *Journal of Tribology*, 111 (1989) 605-613.

[24] C. Kaynak, A. Ankara and T. J. Baker, Initiation and early growth of short fatigue cracks at inclusions, *Materials Science and Technology*, 12 (1996) 421-426.

[25] A. Melander, A finite element study of short cracks with different inclusion types under rolling contact fatigue load, *International Journal of Fatigue*, 19 (1997) 13-24.

[26] D. Nelias, M. L. Dumont, F. Champiot, A. Vincent, D. Girodin, R. Fougeres and L. Flamand, Role of inclusions, surface roughness and operating conditions on rolling contact fatigue, *Journal of Tribology*, 121 (1999) 240-251.

[27] E. Bormetti, G. Donzella and A. Mazzu, Surface and sub-surface cracks in rolling contact fatigue of hardened components, *Tribology Transactions*, 45 (2002) 274-283.

[28] T. A. Harris, *Rolling bearing analysis*, Wiley-Interscience, New York, USA (2001).

[29] Q. Y. Wang, C. Bathias, N. Kawagoishi and Q. Chen, Effect of inclusion on subsurface crack initiation and gigacycle fatigue strength, *International Journal of Fatigue*, 24 (2002) 1269-1274.

[30] S. R. Agha and C. R. Liu, Experimental study on the performance of superfinish hard turned surfaces in rolling contact, *Wear*, 244 (2000) 52-59.

[31] G. Taguchi, Taguchi on robust technology development: Bringing quality engineering upstream, *ASME press* (1993).

[32] G. Bellows, *Low stress grinding for quality production*, Machinability Data Center (1978).
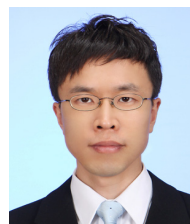
Youngsik Choi is an Assistant Professor of Mechanical Engineering at Chung-Ang University in Seoul, South Korea. He received his Ph.D. degree in industrial engineering from Purdue University. His research interests are in the area of design and manufacturing.